CHEMISTRY OF MATERIALS

Article

pubs.acs.org/cm

Experimental and First-Principles Thermodynamic Study of the Formation and Effects of Vacancies in Layered Lithium Nickel Cobalt Oxides

Yongseon Kim,[†,‡] Doyu Kim,[‡] and Shinhoo Kang[†,*]

[†]Department of Materials Science and Engineering, Seoul National University, Seoul, 151-742, Korea

[‡]SAMSUNG SDI CO., LTD., Yongin-si, Gyeonggi-do, 446-577, Korea

Supporting Information

ABSTRACT: The formation of vacancies and the structural stability of layered lithium nickel oxide (LNO)-based cathode materials are investigated. The thermodynamic stability of oxygen and lithium vacancies and their most stable configurations are examined by first-principles density functional theory calculations. The underlying chemical mechanism is analyzed by a molecular orbital method. The weaker ionic bonding between Ni and O than between Co and O is found to be the main cause for the imperfect structure of LNO crystals. On the basis of these calculations, phase diagrams of the Li−(Ni,Co)−O system were simulated. The crystals containing vacancies are included as independent phases in the simulation. This approach enabled investigation of the relationship between the processing conditions and vacancy formation. The O and Li vacancy pairs are simulated to appear with high temperature processing. On the basis of the calculation of energy barriers, we speculate that these vacancy pairs provide an alternative migration route for Ni ions, which causes the observed structural instability. The effect of oxygen partial pressure was also examined. The first-principles calculation results were compared with experimental results, which showed excellent agreement confirming the validity of the models and calculation methods used in this study.

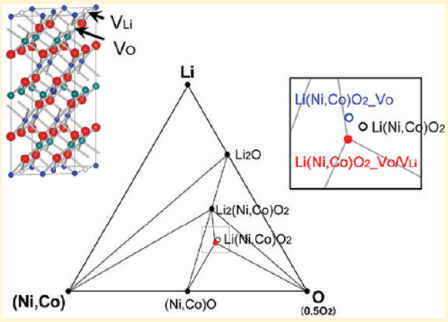

KEYWORDS: *DFT calculations, phase diagrams, molecular orbital method, Lithium ion batteries, cathode materials*

1. INTRODUCTION

Lithium nickel oxide ($LiNiO_2$; LNO) is a promising alternative to $LiCoO_2$ (LCO), which is widely used in lithium ion batteries.[1−5] LNO is isostructural with LCO, whose crystal structure consists of layers of transition metal cations separated from Li layers by oxygen and which belongs to the space group $R\bar{3}m$.[6−10] LNO has several advantages over LCO: it has a higher specific energy, is less toxic, and its raw materials are less expensive. However, there are concerns about its safety, cyclability, and thermal stability.[11−15] These problems must be overcome before LNO can become competitive with other materials and be used in practical devices.

The problems associated with LNO compounds originate mainly from their structural instability.[12,13,16−22] Structurally ordered LNO compounds are known to be difficult to synthesize because Ni^{3+} is not as stable as Co^{3+} in layered structures. Consequently, nonstoichiometric $Li_{1-\delta}Ni_{1+\delta}O_2$ phases usually form. It is reported that excess of Ni ions with an oxidation number of +2 occupy the Li layer by replacing Li ions. These Ni^{2+} ions in the Li sites are expected to disrupt lithium diffusion, thereby reducing the reversible electrochemical capacity.[17,18] Another instability problem originates from the low energy barrier for the migration of Ni ions. The tetrahedral path O_h(octahedral Ni site)−T_d(tetrahedral site)−O_h(octahedral Li site) is reported to have a lower energy barrier than other migration routes.[23−25] According to Ma et al,[26] the height of the migration barrier of Ni is intermediate between those of Mn and Co, which indicates that LNO has an inferior cyclic retention to LCO (although, unlike LMO, it does not rapidly transform into a spinel-like structure).

The mechanism by which the +2 oxidation state of Ni ions causes the instability of LNO is generally explained as follows:[18,26] two Ni^{2+} ions replace a Li^+ ion and a Ni^{3+} ion to maintain charge neutrality. The Ni^{2+} ion, which has a larger ionic size than the Ni^{3+} ion and a similar ionic size to the Li ion, prefers to occupy the octahedral sites in the Li layer. The relatively low migration energy barrier may help Ni ions to reach Li sites. Preparing LNO with an excess amount of Li is effective for forming the stoichiometric composition of LNO. Doping of other metals such as Al, Mg, Co, Mn, and Sb has been investigated and some of them have been found to stabilize the LNO structure.[27−32]

Mixing Co with Ni may be the most effective way to stabilize LNO. $Li(Ni_{1-x}Co_x)O_2$ (LNCO) exhibits less disorder in the sequences of Ni and Li than LNO.[12,19,22] Rougier et al.[19] and Delmas et al.[22] suggested that the substitution of Co, which

Received: August 15, 2011
Revised: November 2, 2011
Published: November 10, 2011

ACS Publications © 2011 American Chemical Society

readily forms the +3 oxidation state and has a larger ionic size than Ni^{3+}, causes the lattice to contract, which destabilizes divalent Ni ions. However, the currently accepted mechanism based on Li/Ni mixing and the effect of Co substitution on ionic size seems to be inadequate. One counter example to this mechanism is the layered structure containing a mixture of Ni, Co, and Mn (LNCM): the oxidation state of the Ni ion in LNCM is close to +2[33,34] and yet the material is used commercially because it has a high structural and thermal stability. We consider that previous studies have placed too much emphasis on the oxidation state of Ni and the ionic size, and they have overlooked the formation of defects such as vacancies and associated effects, even though many studies have found that synthesis in an oxygen-rich atmosphere reduces the number of Ni ions in the Li layers.

The present study focuses on vacancies in LNO and LNCO crystals. The thermodynamic stability of oxygen and lithium vacancies (V_O, V_{Li}) and their most stable configuration are examined by performing first-principles density functional theory (DFT) calculations. The chemical aspects of the calculation results are analyzed by first-principles calculations based on molecular orbital methods. The phase diagram of the Li−(Ni,Co)−O system is simulated as a function of temperature and the effects of the synthetic temperature and oxygen partial pressure on the formation of the vacancies are examined. We show that V_O−V_{Li} pairs, which are found to be the most stable vacancy arrangement in the calculation, can provide a pathway of low energy barrier, thus proposing it as a new migration route of Ni ions to Li sites. The findings of the first-principles investigations are discussed by comparing them with experimental results.

2. METHODS

2.1. First-Principles Calculations. A thermochemical study on vacancies in the LNCO crystal was performed by calculating the formation energies of vacancies with various configurations with respect to their locations by first-principles DFT. The generalized gradient approximation with a correction for the self-interactions of d electrons (the GGA+U method) and plane augmented wave (PAW) pseudopotentials implemented in the Vienna ab initio simulation package (VASP)[35,36] were used with an energy cutoff of 500 eV and a self-consistent field (SCF) convergence of 1×10^{-5} eV. We allowed full relaxation of atomic positions and lattice vectors of $Li_{12}TM_{12}O_{24}$ supercells ($5.766 \times 5.766 \times 14.199$ Å^3) in the structure optimization and the energy calculation (TM = Ni, Co). Because DFT calculations for gas molecules exhibit considerable errors, the chemical potential of the O_2 molecule at room temperature was determined by combining DFT calculations for various metal oxides and experimentally obtained thermochemical data. The effects of temperature and pressure were reflected in the calculations based on the data in JANAF thermochemical tables.[37]

The properties and strengths of the chemical bonds were also analyzed by first-principles discrete variational Xα (DV-Xα) molecular orbital method.[38] This method approximates the exchange−correlation interaction with the Xα potential proposed by Slater[39] and numerically solves the Schrödinger equation using the Hartree−Fock−Slater method. No restriction is imposed on the form of the basis functions because the calculation is conducted numerically; consequently, linear combinations of atomic orbitals (LCAO) can be used without any modification. In addition, this method does not use the pseudopotential approximation; all the atomic orbitals are included in the calculation. This permits reliable information to be obtained regarding the molecular orbitals and the electron distributions.[40−42] The $[Li_6Ni_7O_{14}]$, $[Li_6Ni_6Co_1O_{14}]$, and $[Li_6Co_7O_{14}]$ cluster models were used. The transition metals of interest were located at the center of the clusters to improve the accuracy. The clusters were located at the center of the Madelung field that was generated by translating nine unit cells in each direction.

The Gibbs free energies of all the compounds need to be compared in order to construct a phase diagram because the diagram shows the most stable phases under given conditions. For the phases of the Li−transition metal(TM)−O system, the stability of each phase was determined by comparing the normalized Gibbs free energies, which is expressed by

$$\bar{G}(Li_aTM_bO_c) = \frac{G(T, P, Li_aTM_bO_c)}{a + b + c}$$

Because the PV and the entropy have a negligible effect on the Gibbs free energy for solids,[43,44] this equation can be approximated as

$$\bar{G}(Li_aTM_bO_c) = \frac{G(T, P, Li_aTM_bO_c)}{a + b + c} \approx \frac{E^\circ(0\ \mathrm{K}, Li_aTM_bO_c)}{a + b + c}$$

$$\left(\text{since } G = E + PV - TS = E^\circ(0\ \mathrm{K}) + P^\circ V(0\ \mathrm{K}) + \int_{0\ \mathrm{K}}^{T} C_p dT + \int_{P^\circ}^{P} \{V(1 - \alpha T)\} dP - TS \approx E^\circ(0\ \mathrm{K})\right)$$

For each phase, the position on a ternary diagram (x and y) and the normalized Gibbs free energy (z) represent a unique point in 3-D space. The chemical potential of oxygen ($1/2\ \mu_{O_2}$) can also be located in the same space. Ternary phase diagrams could be obtained by taking vertices and edges which form a convex hull[45] in the $-z$ direction, and projecting them onto a plane. All the compounds of the Li−TM−O system registered in the International Crystal Structure Database (ICSD) were included in this calculation.[46]

The mobility of Ni ions to Li sites was assessed by monitoring the change in energy for various Ni positions. Two routes were examined: one along $O_h \rightarrow T_d \rightarrow O_h$, which has been reported previously, and another new route through an oxygen vacancy ($O_h \rightarrow V_O$ site$\rightarrow O_h$), which is proposed in this study. The same supercell size was used as that used in the vacancy formation calculation ($Li_{12}TM_{12}O_{24}$). Because the mobility is strongly affected by surrounding positive ions,[25,26,47] four configurations of cations near the migration routes were investigated: Li 0% (fully delithiated state), Li 100%, and two kinds of Li 50% states (referred to as Li 50%-configuration 1 and Li 50%-configuration 2).

It is crucial to precisely determine the value of the U parameter to accurately perform GGA+U DFT calculations. Although the GGA+U method is more accurate than the GGA, different values have been reported for the U parameter and it varies depending on the crystal structure and the oxidation state of the transition metals involved.[48−50] Thus, the U parameter should be determined for each system by a process of trial and error so that it reflects the actual material properties. We calculated the energy and the lattice parameter of the LNO crystal for various Li contents and oxidation states of the Ni ion by varying the U parameter and we selected the U parameters for which the DFT calculation results most closely match the experimental data (i.e., the phase transition enthalpy and the variation in the lattice parameter with Li content). Using this process, the optimum U values were found to be 5.0 eV for Ni^{2+} and 6.5 eV for Ni^{4+}, which indicates that the U value increases with increasing oxidation number of Ni ions. We used these U values and applied linear interpolation between these two values to determine the U values of intermediate oxidation states (see the Supporting Information, 1).

To analyze the thermochemistry of an oxide system, we need to accurately calculate the energy changes that occur in the oxidation reaction. However, first-principles calculations often exhibit consid-

dx.doi.org/10.1021/cm202415x | Chem. Mater. 2011, 23, 5388−5397

erable errors because it is difficult to develop appropriate structural models for gaseous phases and the binding energies of atoms are often incorrectly calculated. Furthermore, the GGA produces a large error when O^{2-} is formed from O_2 by adding electrons to p orbitals.[49,50] Yet the overall errors associated with the oxidation reactions can be corrected by just determining the enthalpy of O_2 molecules so that it may include all errors. It is because the overall error values of oxidation reactions are, more or less, fixed regardless of the cations involved.[49] Thus, properly determining the chemical potentials of O_2 can compensate DFT errors and improve the accuracy of calculations for oxidation reactions.

We calculated the energies of metal oxides for various oxidation numbers and compared them with reported experimental standard formation enthalpies. We then determined the enthalpies of oxygen gas molecules by selecting the enthalpies that gave the best agreement between the DFT calculation results and the experimental data (see the Supporting Information, 2). Another potential source of error is that the DFT calculations were performed at 0 K, whereas the standard formation enthalpies were obtained at 298 K. To account for this, the heat capacity difference between metals and their oxides should be integrated between 0 and 298 K and added. However, this error has been reported to be negligible[49] and thus it was neglected. Consequently, the room-temperature enthalpy of O_2 was determined to be −8.95 eV/formula unit. This value was used for all the oxidation reactions in this study. It was adjusted for temperature and pressure using data in the JANAF thermochemical tables.

2.2. Experimental Section. We prepared LNCO cathode materials and observed their properties to assess the validity of our first-principles study. The coprecipitate $(Ni_{0.92}Co_{0.08})(OH)_2$ was obtained by the continuous coprecipitation method and was used as the precursor. Specifically, aqueous solutions of transition metals, NH_4OH, and NaOH were added to a 5 L reactor. The metal solution was prepared by dissolving $NiSO_4{\cdot}6H_2O$ (EP grade; Incheon Chemicals Ltd., Korea) and $CoSO_4{\cdot}7H_2O$ (EP, Nihon Kagaku Ltd., Japan) in deionized water. The solution had a concentration of 1.5 M and the injection rate was 0.1−0.5 mol/h. Commercial NH_4OH solution (28 wt %, Dongwoo Finechem Ltd., Korea) was added to the reactor while maintaining a constant TM/NH_4OH molar ratio. The feed pump of NaOH (99%, OCI Ltd., Korea) solution was connected to a pH sensor/controller and its pumping rate was automatically controlled to maintain a constant pH of 12.3 ± 0.1 inside the reactor. The product slurry overflowed through an outlet and it was washed and dried. The hydroxide precursors were mixed with $LiOH{\cdot}6H_2O$ (99%, Samchun chemical Ltd., Korea). The Li/TM molar ratio of mixing was fixed at 1.03 considering a little evaporation loss of Li. The mixture was heated at 750−850 °C for 15 h under a flow of dry air or oxygen; this ensured that homogeneous LNCO cathode materials were obtained. They were then washed and annealed as necessary.

The morphology of particles and homogeneity of the metals were analyzed using a field-emission scanning electron microscope (FE-SEM; JEOL, 6360F, Japan) and energy-dispersive spectroscopy (EDS). To assess the amount of Li impurities on the surface, we dispersed powders of the cathode materials in water and the pH was measured (Metrohm 827 pH lab, Swiss, measuring accuracy ±0.003pH). Two grams of powder were mixed with 100 g of deionized water and the slurry was stirred for 10 min before measuring the pH. After measurement of the pH, the washed powders were filtered and dried. Composition of these powder samples was analyzed by inductively coupled plasma optical emission spectroscopy (ICP-OES, Perkin-Elmer Optima 5300DV, USA). This method enabled to get exact composition of the bulk samples by removing lithium complexes on the surface. The crystal quality of the LNCO samples was analyzed by powder X-ray diffraction (XRD; Rigaku, D-max 2500, Japan).

3. RESULTS AND DISCUSSION: FIRST-PRINCIPLES CALCULATIONS

3.1. Formation of Vacancies in LNCO. The formation energies of O and Li vacancies in LCNO crystals were calculated. These calculations used the $Li_{12}Ni_{11}CoO_{24}$ supercell in which 8.3% of the Ni is substituted by Co. Because it is known that the introduction of Co improves the stability of LNO crystals, our model contained some Co for practical purposes. The Co atom is located at the center of the supercell. The vacancy formation energies at various locations were calculated and compared.

The formation energies were calculated for when O vacancies were located at positions 1−4 in Figure 1; they are listed in

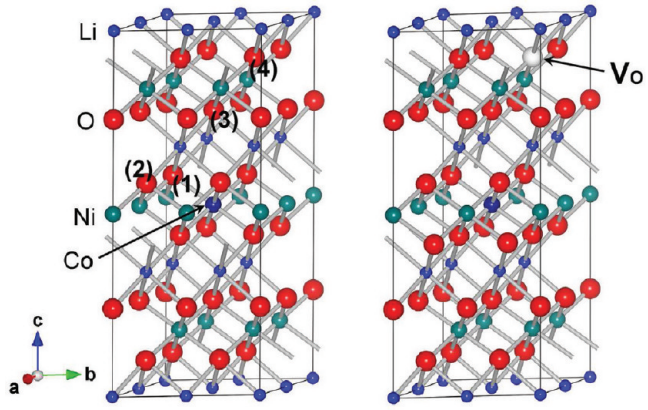

Figure 1. $Li_{12}Ni_{11}CoO_{23}$ (LNCO_V_O) crystal used in energy calculations with an O vacancy in different positions (positions 1−4 in the left figure) and the V_O position at the lowest formation energy (right).

Table 1a. Position 4 was the most stable site for an O vacancy as it has the lowest formation energy. The formation energy increases as the O vacancy becomes closer to the central Co ion. The only exception to this trend is position 1, which is the closest oxygen site to the Co ion. This is presumably due to structural characteristics of the Co-doped LNO crystal: in the structure-optimized LNO crystal, the Li−O and O−Ni bond lengths were found to be 2.033 and 1.997 Å, respectively. The interatomic distances for Li−O and O−Co were, respectively, 2.070 and 1.924 Å in Co-doped LNO (LNCO). This shows that Co substitution causes neighboring O atoms to move closer to Co ions. This distortion of the O positions may increase the strain energy, which would be relaxed by the formation of an O vacancy in the vicinity of the Co ion, reducing the vacancy formation energy and causing the exception to the trend.

The chemical properties of Ni−O and Co−O bonds in the LNCO were analyzed by the DV-Xα molecular orbital method to investigate why the preferred position for an O vacancy is far from the Co ion. Table 2 shows the calculated effective charges of ions. It shows that the Co ion is more positive than the Ni ion, indicating that the ionic bonding of Co−O is stronger than that of Ni−O. This implies that a longer distance between an O vacancy and a Co ion is more favorable because of the Coulomb interaction. The covalent properties of the bonds were examined by calculating bond overlap populations (BOPs). Figure 2 shows overlap population (OP) diagrams for Ni−O and Co−O bonds. Integration of the populations under the highest occupied molecular orbital (HOMO level) gives BOP values for bonding and antibonding orbitals (shown in the figure), which are a measure of covalency. The molecular orbitals of Ni−O and Co−O exhibit similar features in the energy range of the TM 3d−O 2p interaction, although the

dx.doi.org/10.1021/cm202415x | Chem. Mater. 2011, 23, 5388−5397

Table 1. Calculated Energies of Supercells with Vacancies in Various Positions. Energies of (a) $Li_{12}Ni_{11}CoO_{23}$ (LNCO_V_O) for an O Vacancy in Different Positions and (b) $Li_{11}Ni_{11}CoO_{23}$ (LNCO_V_O/V_{Li}) for a Li Vacancy in Different Positions (V_O was fixed at position 4 in Figures 1 and 3)

position of V_o	V_o–Co distance (Å)	energy (per supercell, eV)
1	1.924	−19.1845
2	3.402	−19.1466
3	3.724	−19.1473
4	6.004	−19.1992
position of V_{Li}	V_{Li}–V_O distance (Å)	energy (per supercell, eV)
1	2.033	−18.8398
2	3.441	−18.7917
3	4.477	−18.7910
4	6.753	−18.7622

Table 2. Effective Charge of Ions in LNCO, LNO, and LCO Crystals Calculated by DV-Xα Molecular Orbital Method

	LNCO	LNO	LCO
Li	+0.875	+0.872	+0.917
O	−0.934	−0.929	−1.118
Ni	+1.152	+1.155	
Co	+1.485		+1.372

covalent bonding of Co−O appears to be slightly stronger than that of Ni−O because the antibonding orbitals of Co−O are located at slightly higher energies than those of Ni−O. Thus, stable locations for O vacancies are mainly determined by the difference in the ionic interactions of Co−O and Ni−O. Table 2 also lists the calculated effective charges of ions in pure LNO and LCO for reference. The ions were more ionized in LCO. The higher operation voltage of the LCO cathode seems to be due to the stronger ionic bonding of Li−O in the LCO crystal than in the LNO crystal.

A Li vacancy is considered to be formed in addition to an O vacancy since the coexistence of both vacancies may be favorable for maintaining the charge neutrality of the crystal. Figure 3 shows calculation of formation energies for Li vacancies at positions 1−4 when there is an O vacancy at position 4 in Figure 1 (i.e., the most stable position). The result shows that the formation of a Li vacancy close to the O vacancy is favored (Table 1b). The stable locations for a Li vacancy also appear to be determined by the ionic interaction energy: because the Li−O bond is highly ionic in character, a short distance between the Li and O vacancies may minimize the Coulomb interaction energy.

The formation of only V_{Li} or V_{Ni} seems to be improbable because it is not consistent with experimental results that reported that the LNO composition depends on the synthetic atmosphere and that Ni-rich compounds are generally formed. We examined the Li vacancy because it provides insight into the formation mechanism of vacancy pairs. Energy calculations of supercells containing a V_{Li} revealed that V_{Li} is more stable at position 1 in Figure 3, which is distant from the Co ion, than at position (3) (−19.347 and −19.246 eV/supercell, respectively). This agrees with the above calculation, which indicates that a V_O–V_{Li} pair prefers to be far from the Co ion. Formation of V_{Li} may be expressed as follows

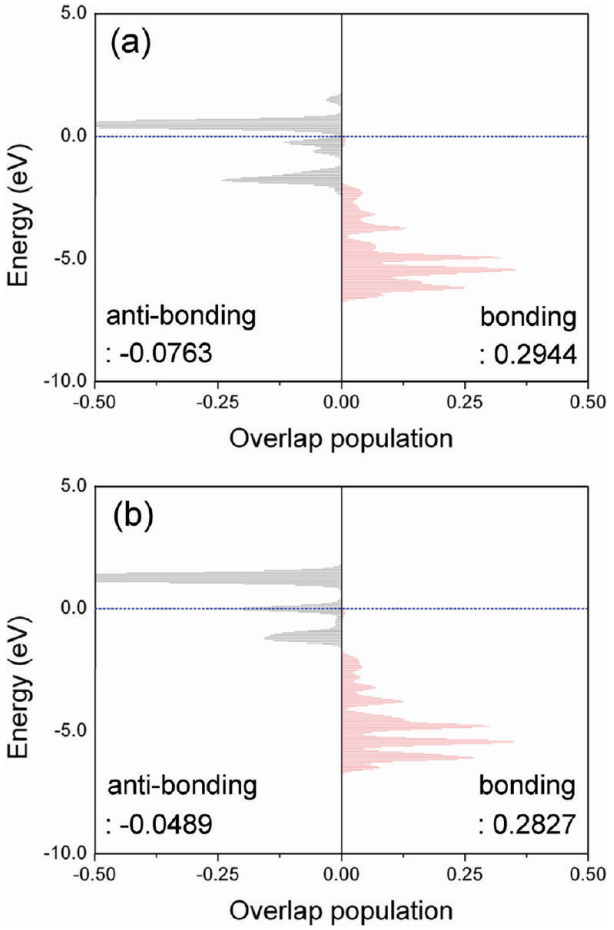

Figure 2. OP diagrams of (a) Ni−O bond and (b) Co−O bond calculated by DV-Xα molecular orbital method. The left and right sides respectively show OP of bonding and antibonding orbitals together with BOP values.

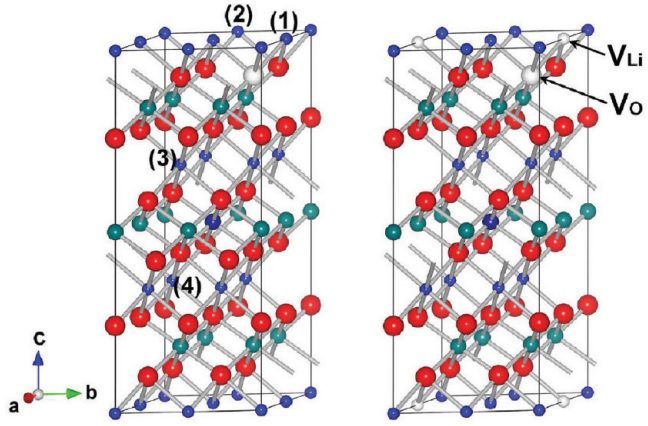

Figure 3. $Li_{11}Ni_{11}CoO_{23}$ (LNCO_V_O/V_{Li}) crystal used in energy calculations with a Li vacancy in different positions (positions 1−4 in the left figure) when there is an O vacancy, and the V_O and V_{Li} configuration for the lowest formation energy (right).

$$Li_{12}TM_{12}O_{24} + \frac{1}{4}O_2 = Li_{11}TM_{12}O_{24} + \frac{1}{2}Li_2O$$

This process may be considered to be a part of the inverse reaction to the synthesis of LNCO. During the synthesis, Li

dx.doi.org/10.1021/cm202415x | Chem. Mater. 2011, 23, 5388–5397

sites distant from the Co ion will remain empty at low temperatures, whereas those close to the Co ion are filled. There may be a deficiency of oxygen ions during synthesis at long distances from the Co ion and close to V_{Li}s (if they exist) because the energy of V_O decreases with increasing distance from Co and it compensates the destruction of charge neutrality caused by V_{Li} formation. Thus, V_O or a V_O−V_{Li} pair may be formed by these mechanisms during firing.

3.2. Phase Equilibria of LNCO Containing Vacancies.

The previous section showed that an O vacancy in LNCO is stable when it is located far from Co ions. When Li vacancies coexist, they prefer to be close to O vacancies. The vacancy formation reactions in $Li_{12}Ni_{11}CoO_{24}$ supercell can be expressed by following equations (eq 1.1 is for formation of V_O and eq 2.1 is for formation of a V_O−V_{Li} pair); changes in the Gibbs free energy of these reactions at the standard state can be obtained from eqs 1.2 and 2.2 and the vacancy formation temperature can be calculated using eq 1.3 and 2.3, respectively.

The effects of the PV and entropy in solids were omitted because they are negligible compared to other factors.[49,50] Thus, the approximations expressed by eq 1.2 and 2.2 seem reasonable.

$$Li_{12}TM_{12}O_{24} \rightarrow Li_{12}TM_{12}O_{23} + \frac{1}{2}O_2(g) \quad (1.1)$$

$$\begin{aligned}\Delta G^\circ &= G^\circ(Li_{12}TM_{12}O_{23}) + \frac{1}{2}G^\circ(O_2) \\ &\quad - G^\circ(Li_{12}TM_{12}O_{24}) \\ &\cong E^\circ(Li_{12}TM_{12}O_{23}) + \frac{1}{2}\{H^\circ(O_2) - TS^\circ(O_2)\} \\ &\quad - E^\circ(Li_{12}TM_{12}O_{24})\end{aligned} \quad (1.2)$$

$$\begin{aligned}T_f &= (2\{E^\circ(Li_{12}TM_{12}O_{23}) - E^\circ(Li_{12}TM_{12}O_{24})\} \\ &\quad + H^\circ(O_2))/(S^\circ(O_2))\end{aligned} \quad (1.3)$$

$$\begin{aligned}Li_{12}TM_{12}O_{24} \rightarrow Li_{11}TM_{12}O_{23} + \frac{1}{2}Li_2O \\ + \frac{1}{4}O_2(g)\end{aligned} \quad (2.1)$$

$$\begin{aligned}\Delta G^\circ &= G^\circ(Li_{12}TM_{12}O_{24}) + \frac{1}{2}G^\circ(Li_2O) \\ &\quad + \frac{1}{4}G^\circ(O_2) - G^\circ(Li_{12}TM_{12}O_{24}) \\ &\cong E^\circ(Li_{12}TM_{12}O_{23}) + \frac{1}{2}E^\circ(Li_2O) \\ &\quad + \frac{1}{4}\{H^\circ(O_2) - TS^\circ(O_2)\} \\ &\quad - E^\circ(Li_{12}TM_{12}O_{24})\end{aligned} \quad (2.2)$$

$$\begin{aligned}T_f &= (4\{E^\circ(Li_{12}TM_{12}O_{23}) - E^\circ(Li_{12}TM_{12}O_{24})\} \\ &\quad + 2E^\circ(Li_2O) + H^\circ(O_2))/(S^\circ(O_2))\end{aligned} \quad (2.3)$$

The O vacancy formation temperatures for $Li_{12}Ni_{12}O_{24}$ (LNO) and $Li_{12}Co_{12}O_{24}$ (LCO) supercells were respectively calculated to be ~1100 and 3500 K at the standard state. This indicates that O vacancies can be formed at relatively low temperatures in LNO, whereas high temperature over 3500 K is needed in LCO. For Co-doped LNO ($Li_{12}Ni_{11}CoO_{24}$, LNCO), the temperature increased to 1300 K, higher than that of pure LNO. This indicates that the substitution of Co for Ni suppresses the formation of O vacancies. It has been reported to be difficult to synthesize pure LNO with a high structural quality and Co and/or Mn should be added to improve the stability of LNO crystals. Our calculation results imply that Co stabilizes the structure because it makes the formation of O vacancies in the system difficult by providing a strong ionic bond. The temperatures of O vacancy formation at positions 1, 2, and 3 in Figure 1 were respectively calculated to be 1450, 1750, and 1750 K, indicating that higher temperatures are required to form O vacancies at these positions than at position 4.

The temperature of V_O−V_{Li} vacancy pair formation in LNCO was also calculated using eq 2.3. For the configuration with the lowest formation energy (Figure 3, right) the V_O−V_{Li} formation temperature was ~1300 K, which is similar to that for single O vacancy formation. The vacancy pair formation temperatures for positions 2−4 in Figure 3 were respectively calculated to be 2150, 2150, and 2650 K, which are much higher than that of position 1 (the most stable position). These equilibrium temperatures calculated using eqs 1.3 and 2.3 do not represent the exact vacancy formation temperatures since the thermodynamic stabilities of vacancy-containing phases must be compared with those of other possible phases. In addition, the similar formation temperatures for a single O vacancy and a V_O−V_{Li} pair make it difficult to verify what kind of vacancies form in actual LNCO crystals. Thus, a more systematic investigation on the phase diagrams of the Li−(Ni,Co)−O system is required.

Figure 4 shows the phase diagrams of the Li−(Ni,Co)−O system obtained from the simulation by assuming an oxygen partial pressure of 0.02 MPa (in air). The Co/(Ni+Co) ratio was fixed at 1/12. A mixed state of Ni and Co was considered rather than pure Ni because we are more interested in the LNCO phase, which is used in practical applications. Along with all the reported compounds of the Li−(Ni,Co)−O system, we included $Li_{12}CoNi_{11}O_{23}$ (LCNO_V_O) and $Li_{11}CoNi_{11}O_{23}$ (LCNO_V_O/V_{Li}), which are LNCO systems respectively containing V_O and V_{Li}+V_O, as independent phases in the calculation. This analysis is expected to show what type of defects can exist stably under certain conditions. (Supporting Information 3 shows the energy calculation results for Li−(Ni,Co)−O compounds, including LNCO, LNCO_V_O, and LNCO_V_O/V_{Li}, which were used in the calculation.)

Figure 4a shows the room-temperature ternary phase diagram simulated. Li_2O, (Ni,Co)O, $Li_2(Ni,Co)O_2$, $Li(Ni,Co)O_2$, and $Li(Ni,Co)_2O_4$ appear as stable phases that make up a convex hull. Points 1 and 2 in Figure 4a respectively denote the positions of LNCO_V_O and LNCO_V_O/V_{Li}. LNCO without any vacancies and LNCO_V_O/V_{Li} (point 2) exist as stable phases, whereas LNCO_V_O (point 1) does not. This calculation results indicate that a Li−O vacancy pair is more stable than a single O vacancy at room temperature. When the temperature is increased to 1100K (Figure 4b), perfect LNCO no longer exists on the convex hull, whereas LNCO_V_O/V_{Li} is still stable. It seems that LNCO containing V_O/V_{Li} pairs will be formed instead of a perfect LNCO crystal because of the low oxygen chemical potential at temperatures higher than 1100K. At 1500K, even LNCO_V_O/V_{Li} disappeared, indicating that neither perfect LNCO nor LNCO with vacancies are stable at

dx.doi.org/10.1021/cm202415x | Chem. Mater. 2011, 23, 5388−5397

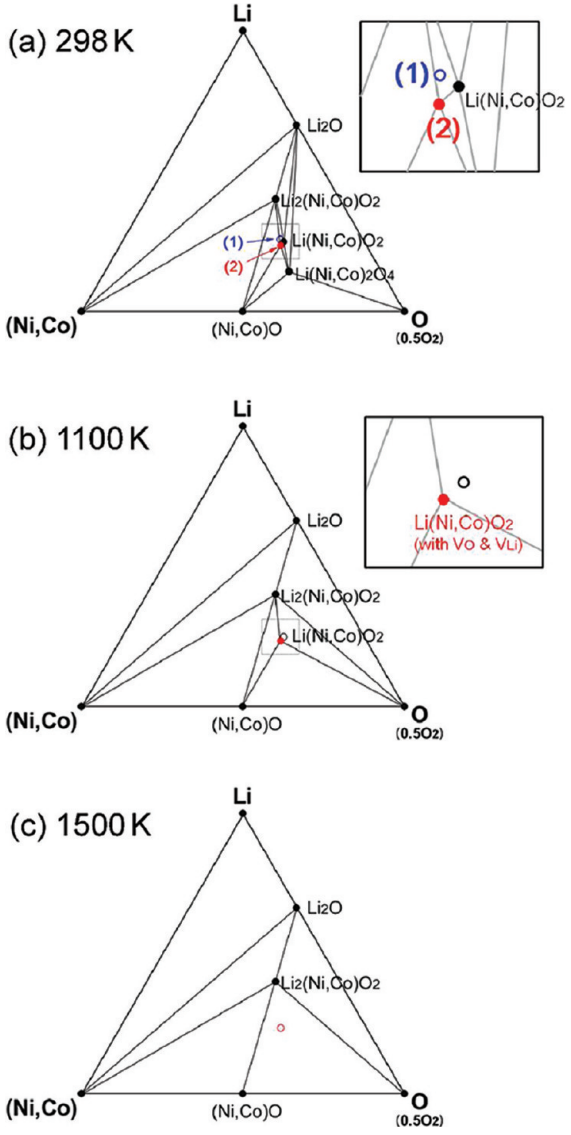

Figure 4. Phase diagrams of Li−(Ni,Co)−O system determined by DFT calculations. (1) and (2) indicate positions of LNCO_V_O and LNCO_V_O/V_{Li}, respectively.

this temperature. LNCO with more vacancies may form or the phases may decompose into $Li_2(Ni,Co)O_2$, (Ni,Co)O, and O_2 above 1500 K.

The calculated phase transition temperatures may not agree with experimentally measured ones. In addition, vacancy concentrations (i.e., 4.2 and 8.3% for V_O and V_{Li}, respectively; i.e.,1 O atom missing out of 24 atoms and 1 Li atom missing out of 12 atoms, respectively) maybe unrealistic, resulting in errors in the transition temperatures in Figure 4, which depend on the vacancy concentrations. Nevertheless, the overall tendency that LNCO_V_O/V_{Li} is more stable than perfect LNCO at high temperatures is expected to be valid.

3.3. Ni to Li Site: Migration Barriers and Stability.

Phase transformations from the layered structure to other structures are undesirable because they cause poor cyclic and thermal stability. Delithiated LCNO is thermodynamically unstable and consequently kinetic stability is required. The migration of Ni ions to Li sites should be suppressed to prevent the phase transformation from the layered structure to spinel or rock-salt phases by maintaining the kinetic stability. The migration energy barriers for a Ni ion to Li sites were calculated to examine the effect of vacancy formation on the phase stability. The migration via adjacent tetrahedral sites has been reported to be the main route because it has the lowest energy barrier.[25,26] Although it is not the shortest distance, this route provides a larger separation between migrating Ni and O ions than other routes, which minimizes the interactions between the ions during migration.

The formation of a V_O−V_{Li} pair alters the arrangement of Ni−O−Li to Ni−V_O−V_{Li}. The space formed by an oxygen vacancy probably provides an alternative migration path for Ni ions (see Figure 5b). We calculated the migration energy barriers of two routes: the conventional O_h(Ni)→T_d→O_h(Li) route (Figure 5a) and another O_h(Ni)→V_O site→O_h(Li) route proposed in this study (Figure 5(b)), where O_h and T_d denote octahedral and tetrahedral sites, respectively. Three different cation configurations were used: Li 100%, Li 50% (half delithiated), and Li 0% (fully delithiated). In the Li 100% configuration, because there is no vacant Li site for a Ni ion to enter, we simultaneously translated Li and Ni ions so that they eventually exchange positions. Li 50% was again divided into two configurations with different Li ion distributions near the migration channels.

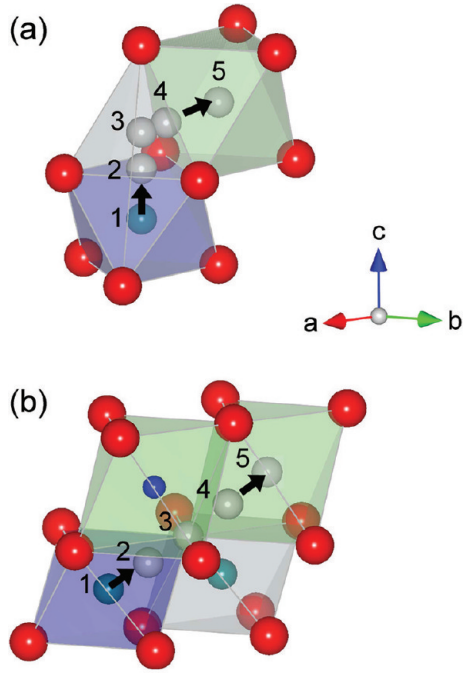

Figure 5. Migration routes of Ni ions to Li sites in the layered structure for (a) the O_h→T_d→O_h route and (b) the O_h→V_O site→O_h route.

The calculation results for the O_h(Ni)→T_d→O_h(Li) route are plotted in Figure 6a. The *x*-axis in Figure 6 represents the positions of Ni ions along the path, which are indicated in Figure 5. The energy barrier appears to vary depending on the cation configuration. Table 3a lists the number of nearest cations and their distance from the T_d and O_h(Li) sites together with the magnitude of the energy barrier at the positions. The energy barrier when a Ni ion passes through a T_d site was inversely proportional to the number of nearest cations. This implies that the main factor that determines the migration barrier is the Coulomb repulsion from the surrounding cations.

dx.doi.org/10.1021/cm202415x | *Chem. Mater.* 2011, 23, 5388–5397

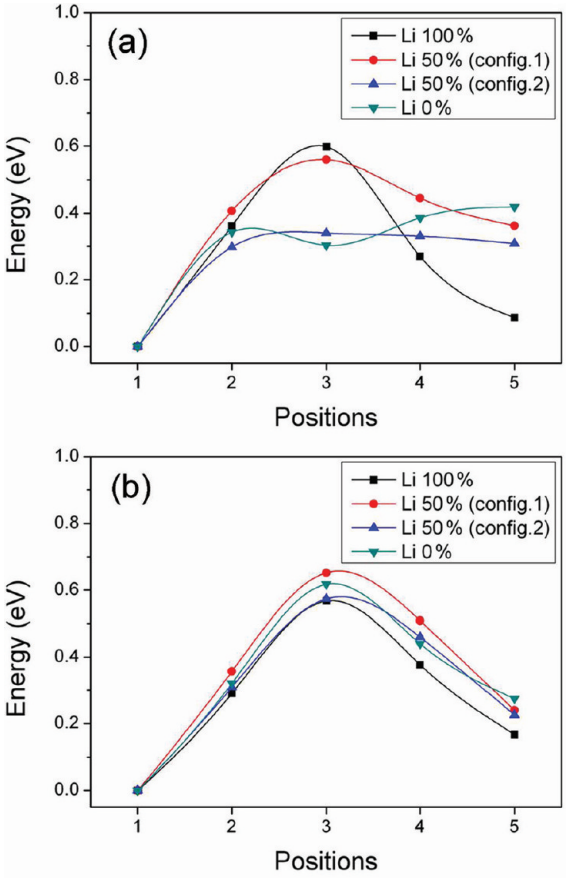

Figure 6. Energy barriers calculated for migration of a Ni ion for (a) the $O_h \rightarrow T_d \rightarrow O_h$ route and (b) the $O_h \rightarrow V_O$ site$\rightarrow O_h$ route. The *x*-axis denotes the positions of Ni ions on the migration paths in Figure 5.

Ni ion migration through the $O_h(Ni) \rightarrow T_d \rightarrow O_h(Li)$ route is greatly facilitated for Li 0% and Li 50% (configuration 2) because of the low energy barriers, which may cause a phase transformation and degradeation of performance.

The migration barrier for the $O_h(Ni) \rightarrow V_O$ site$\rightarrow O_h(Li)$ route was affected little by the configuration of surrounding cations while that of $O_h(Ni) \rightarrow T_d \rightarrow O_h(Li)$ was strongly dependent (Figure 6b and Table 3b). This is presumably because two of the four nearest cations of the V_O sites are Ni ions, which have large effective charges. The Coulomb repulsion of these two Ni ions seems to be sufficiently large to nullify the influence of the remaining Li ions. The energy barriers have a maximum in the range 0.567−0.652 eV when Ni ions pass through the V_O sites. Those values are almost equivalent to those for the $O_h(Ni) \rightarrow T_d \rightarrow O_h(Li)$ route (0.560−0.598 eV) for Li 100% and Li 50% (configuration 1), but it is much larger than 0.303−0.340 eV for Li 50% (configuration 2) and Li 0%.

Based on all these results, the $O_h \rightarrow T_d \rightarrow O_h$ and $O_h \rightarrow V_O$ site$\rightarrow O_h$ routes are expected to provide similar probabilities for Ni migration in the Li 100% and Li 50% configurations in which relatively many Li ions are located near the migration routes. For Li 0% and Li 50% (config. 2) with less Li ions near the T_d site, migration of Ni through $O_h \rightarrow T_d \rightarrow O_h$ will prevail because of lower energy barrier. However, the Ni ions are less stable at Li sites (O_h(Li) sites), thus the possibility of reverse migration ($O_h(Li) \rightarrow T_d \rightarrow O_h(Ni)$) may not be ignored. In conclusion, the new $O_h \rightarrow V_O$ site$\rightarrow O_h$ route proposed in this study is expected to provide comparable probability of Ni ions' migration path to the conventional $O_h \rightarrow T_d \rightarrow O_h$ route under certain conditions, especially when there are many lithium ions near the T_d site. This implies that the formation of V_O−V_{Li} pairs may play a role in causing instability of the LNCO phase.

3.4. Effect of Oxygen Partial Pressure. The findings in the previous section suggest that minimizing the vacancy formation and synthesizing LNCO under high oxygen partial pressure will increase the stability of the LNCO phase. Vacancy formation can be minimized by reducing the synthetic temperature (the −TS term in the Gibbs free energy) and/or by increasing the oxygen partial pressure during the reaction. However, the firing temperature must exceed a certain value to ensure completion of the chemical reactions and good crystallinity. Therefore, the most appropriate strategy is to perform synthesis under a high oxygen partial pressure for a given processing temperature.

We calculated the phase diagrams in the same manner as for Figure 4 but using a higher oxygen partial pressure of 0.1 MPa. The shape remained the same, but the transition temperatures differed from those in Figure 4. When p_{O_2} = 0.02 MPa, the perfect LNCO phase became unstable at 1100 K and only LNCO_V_O/V_{Li} was stable in the phase diagram; this transition temperature increased to 1200K for p_{O_2} = 0.1 MPa. Theoretically, the free energy of oxygen decreases by 0.25 eV when the temperature is increased from 1100 to 1200K under p_{O_2} = 0.02 MPa. If p_{O_2} is increased to 0.1 MPa at 1200 K, the free energy again increases by 0.17 eV, which may compensate a considerable portion of the change caused by the increase of temperature: Increasing the oxygen partial pressure from 0.02 to 0.1 MPa is expected to compensate for a temperature increase of 60−70 K.

Table 3. Cation Distribution near the Migration Routes of Ni Ions to Li Sites and Calculated Energy Barriers (maximum energy gain when a Ni ion passes along the routes shown in Figure 5) for Various Li Configurations: (a) Route via Tetrahedral Sites ($O_h(Ni) \rightarrow T_d \rightarrow O_h(Li)$) and (b) Route via O Vacancies ($O_h(Ni) \rightarrow V_O$ site$\rightarrow O_h(Li)$)

	T_d site	$\Delta E(T_d)$	O_h(Li) site	$\Delta E(O_h)$
Li 100%	3 (3 × Li, 1.748 Å)	0.598	9 (4 × Li, 5 × Ni, 2.883−2.893 Å)	0.087
Li 50% (conf. 1)	2 (2 × Li, 1.748 Å)	0.560	7 (2 × Li, 5 × Ni, 2.883−2.893 Å)	0.362
Li 50% (conf. 2)	1 (1 × Li, 1.748 Å)	0.340	7 (2 × Li, 5 × Ni, 2.883−2.893 Å)	0.309
Li 0%	0	0.303	5 (5 × Ni, 2.893 Å)	0.418
	V_O site	ΔE	O_h(Li) site	ΔE
Li 100%	4 (2 × Li, 2 × Ni 1.976−2.113 Å)	0.567	9 (3 × Li, 6 × Ni, 2.883−2.893 Å)	0.167
Li 50% (conf. 1)	4 (2 × Li, 2 × Ni, 1.976−2.113 Å)	0.652	8 (2 × Li, 6 × Ni, 2.883−2.893 Å)	0.240
Li 50% (conf. 2)	3 (1 × Li, 2 × Ni, 1.976−2.113 Å)	0.574	8 (2 × Li, 6 × Ni, 2.883−2.893 Å)	0.226
Li 0%	2 (2 × Ni, 1.976 Å)	0.617	6 (6 × Ni, 2.893 Å)	0.275

dx.doi.org/10.1021/cm202415x | *Chem. Mater.* 2011, 23, 5388−5397

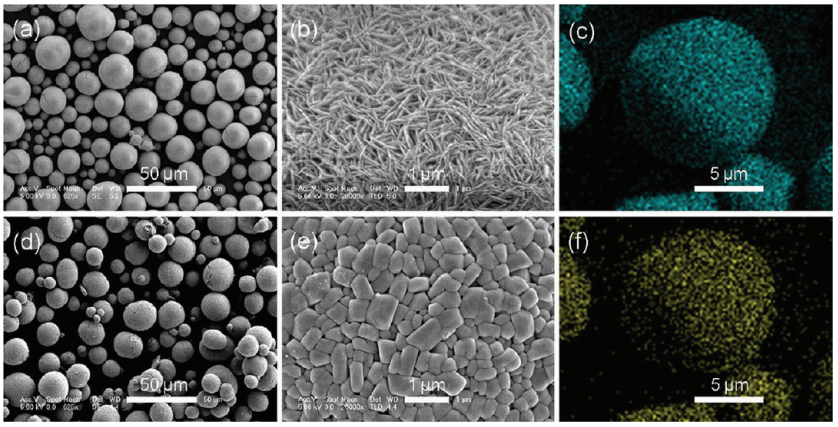

Figure 7. (a, b) SEM images of $(Ni_{0.92}Co_{0.08})(OH)_2$ coprecipitate and (d, e) the LNCO cathode material synthesized from $(Ni_{0.92}Co_{0.08})(OH)_2$. (c, f) Ni and Co distributions obtained by EDS mapping.

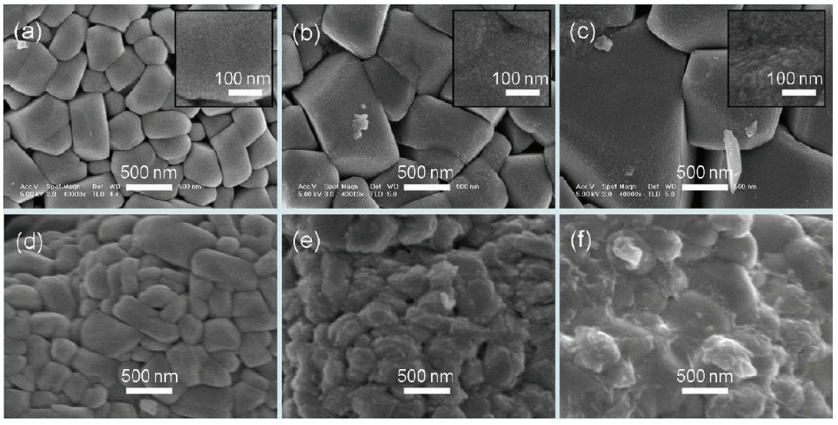

Figure 8. SEM images of LNCO surfaces fired at different temperatures: (a–c) fired at 750, 800, and 850 °C, respectively, and (d–f) annealed at 600, 700, and 800 °C, respectively, after washing of sample a.

4. RESULTS AND DISCUSSION: EXPERIMENTAL RESULTS

Figures 7 and 8 show SEM images of (Ni,Co) hydroxide coprecipitates prepared in this study and the LNCO cathode materials synthesized from them. The coprecipitates exhibit a spherical morphology with a high density (Figure 7a). EDS mapping revealed that the transition metals are uniformly distributed (Figure 7b, c). Figure 8 shows SEM images of surfaces of LNCO samples synthesized at different firing temperatures. It shows that some impurities appear on the surface as the firing temperature is increased (Figure 8a,c). These impurities could be removed by washing in water, but they reappeared when washed samples were annealed at a high temperature (Figure 8d–f). Qualitative analysis by several techniques revealed that the surface impurities were lithium compounds such as Li_2CO_3 and LiOH.

These results support the calculation results presented in sections 3.1 and 3.2, which predicted the formation of both V_O and V_{Li}. The water-soluble impurities, LiOH and Li_2CO_3, may have been formed by reactions between Li or Li_2O (which existed separately on the surface at high temperatures, remaining vacancies in the bulk) and CO_2 or H_2O after high-temperature treatment. Hexagonal plates of $Li_2(Ni,Co)O_2$ crystals appeared on the surface after the washed samples were annealed at a much higher temperature (see the Supporting Information, 4). This is consistent with the calculation results, which predicted that perfect LNCO would decompose into $Li_2(Ni,Co)O_2$, O_2, and LCNO_V_O/V_{Li} at high temperatures (Figure 4). As the temperature decreases, the Li_2O–LNCO_V_O/V_{Li} line instead of the $Li_2(Ni,Co)O_2$–O_2 line becomes stable, composing the convex hull, and the LNCO composition comes to lie in the Li_2O–O_2–LNCO_V_O/V_{Li} triangle. This is why Li_2O rather than $Li_2(Ni,Co)O_2$ was formed on the surface at synthesis temperatures under 850 °C.

Precise quantitative analysis of the lithium compounds on the surface was difficult because they are composed of light elements and the amounts were very small. We washed powder samples and measured the pH of the water to assess the amount of Li compounds, which is expected to be proportional to the V_{Li} concentration in LNCO. This method should be reasonably accurate because aqueous solutions of Li_2CO_3 or LiOH have high alkalinities. Moreover, the pH is an important check point of cathode materials in industry, thus measurement of pH is practically useful. The pH increased with increasing synthesis temperature (Figure 9), indicating that the amount of Li impurities on the surface increase. This result supports the first-principles calculations, which predict that a higher heating temperature will generate more amounts of O and Li vacancies in the bulk and form proportional amount of Li compounds on the surface.

We prepared samples with different Co/(Co+Ni) ratio and measured the pH of them. The pH decreased with increase of the Co content (Figure 10). The composition of the washed powders analyzed by ICP-OES method is also presented in

dx.doi.org/10.1021/cm202415x | *Chem. Mater.* 2011, 23, 5388–5397

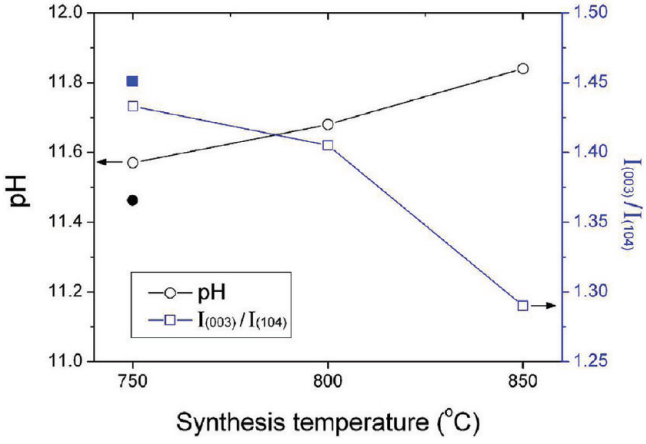

Figure 9. pH (circles) and $I_{(003)}/I_{(104)}$ XRD peak ratio (squares) of LNCO synthesize at different temperatures in air (p_{O_2} = 0.02 MPa, open symbols). The solid symbols indicate the values for LNCO synthesized under 100% oxygen (p_{O_2} = 0.1 MPa) at 750 °C.

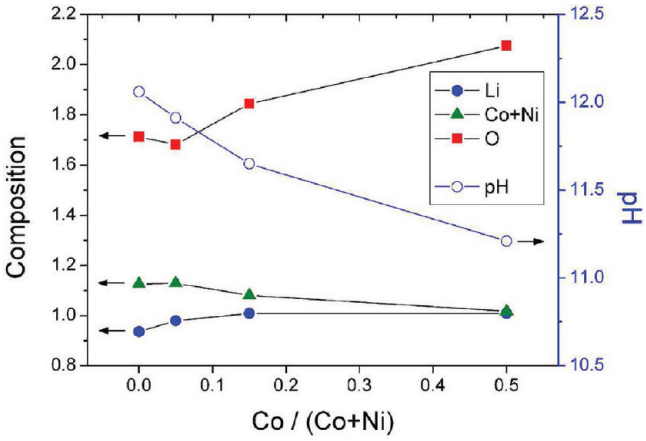

Figure 10. Composition of LNCO samples with different Co content analyzed by the ICP-OES method (solid symbols). pH of the samples are presented together (empty circles). All the samples were synthesized under same firing condition (at 800 °C in air).

Figure 10, which shows that Li and O are deficient in LNCO. The composition approached to that of the ideal $LiTMO_2$ with increase of the Co content. The results indicate that V_O and V_{Li} coexist in the crystal and the concentration could be reduced with increase of the Co content. The pH appeared to be in inverse proportion to Li content of the bulk in Figure 10, which supports the pH could be a useful measure for V_{Li} concentration. Only a trace of other metals except Li were detected from the water used for washing, indicating that the pH is mainly determined by the concentration of Li compounds such as Li_2CO_3 or LiOH which are water-soluble (solubility of Li_2CO_3 and LiOH is reported to be 1.32 and 1.28 g per 100 mL of water at 20 °C, respectively, thus our washing condition seems to have provided enough water to dissolve them on the surface).

The $I_{(003)}/I_{(104)}$ ratio in XRD patterns (the XRD patterns are provided in the Supporting Information, 5) is known to reflect the degree of cation ordering (often called cation mixing).[51] This ratio decreased with increasing synthesis temperature from 750 to 850 °C (Figure 9), which indicates that the cations became more disordered with increasing temperature. The formation of vacancies at high temperatures might be the reason, because the V_O–V_{Li} pair vacancies provide an alternative migration route and residence sites for Ni ions in the Li layer, as discussed in section 3.3. In support of this interpretation, data for the sample synthesized under a 100% oxygen atmosphere (p_{O_2} = 0.1 MPa) is also shown in Figure 9 (solid symbols). The $I_{(003)}/I_{(104)}$ ratio increased and the pH decreased with increasing oxygen partial pressure. This result clearly demonstrates that vacancy formation affects the crystallinity and can be controlled by oxygen pressure.

5. CONCLUSIONS

Previously, the structure and stability of layered lithium nickel oxide have been mostly explained in terms of the oxidation number of Ni ions. In contrast, we focused on vacancy formation and its effect by performing first-principles calculations in the present study. The formation of oxygen and lithium vacancies was found to be thermodynamically more favorable in LNO than in LCO. Doping LNO with Co was found to be effective in preventing vacancy formation. The O vacancy preferred to be far from Co. Analysis by the molecular orbital method revealed that Ni–O has weaker ionic bond strength than Co–O. This indicates that strong ionic bonding is the main cause for the greater structural stability of LCO over LNO and for the reason why Co doping improves the stability of LNO.

The coexistence of O and Li vacancies was favored and their pairing within the shortest distance could increase the thermodynamic stability because of the charge neutrality of the crystal and the strong ionic character of Li–O bonding. The calculated phase diagram showed that both a perfect crystal of LNCO ($Li_{12}Ni_{11}CoO_{24}$) and LNCO with a V_O and V_{Li} (LNCO_V_O/V_{Li}) exist stably at room temperature, but that only LNCO_V_O/V_{Li} is stable above 1100 K. This indicates that vacancies should form easily at high temperatures. The mobility of Ni ions, which is the main factor in causing structural and thermal instability, was assessed by calculating the migration energy barrier. The barrier of the O_h–V_O–O_h route proposed in this study was comparable to that of the conventional O_h–T_d–O_h route, implying the vacancy formation provides alternative route for Ni ion migration. The first-principles calculation results agreed well with the experimental results.

■ ASSOCIATED CONTENT

Supporting Information

Determination of the U parameter for the GGA+U calculation; determination of oxygen chemical potential; energy calculation results for Li–(Ni,Co)–O compounds; SEM image of the LNCO sample that was washed and annealed at a high temperature; XRD patterns of LNCO samples synthesized with various heating conditions; formation energy of V_O with respect to Li concentration. This material is available free of charge via the Internet at http://pubs.acs.org.

■ AUTHOR INFORMATION

Corresponding Author

*Telephone: 82-2-880-7167. Fax: 82-2-884-1578. E-mail: shinkang@snu.ac.kr.

■ REFERENCES

(1) Thomas, M.; David, W.; Goodenough, J.; Groves, P. *Mater. Res. Bull.* **1985**, *20*, 1137.

(2) Dahn, J. R.; Von Sacken, U.; Juzkow, M. W.; Al-Janaby, H. *J. Electrochem. Soc.* **1991**, *138*, 2207.
(3) Broussely, M.; Perton, F.; Labat, J.; Staniewicz, R. J.; Romero, A. *J. Power Sources* **1993**, *43*−*44*, 209.
(4) Ohzuku, T.; Ueda, A. *Solid States Ionics* **1994**, *69*, 201.
(5) Winter, M.; Besenhard, J.; Spahr, M.; Novak, P. *Adv. Mater.* **1998**, *10*, 725.
(6) Johnston, W.; Heikes, R.; Sestrich, D. *J. Phys. Chem. Solids* **1958**, *7*, 1.
(7) Orman, H.; Wiseman, P. *Acta Crystallogr.* **1984**, *40*, 12.
(8) Hewston, T.; Chamberland, B. *J. Phys. Chem. Solids* **1987**, *48*, 97.
(9) Reimers, J.; Li, W.; Dahn, J. *Phys. Rev. B* **1993**, *47*, 8486.
(10) Arroyo y de Dompablo, M.; Ceder, G. *J. Power Sources* **2003**, *119*−*121*, 654.
(11) Ohzuku, T.; Ueda, A.; Kouguchi, M. *J. Electrochem. Soc.* **1995**, *142*, 4033.
(12) Arai, H.; Ijadam, S.; Sakurai, Y.; Yamaki, J. *Solid State Ionics* **1998**, *109*, 295.
(13) Stoyanova, R.; Zhecheva, E.; Alcántara, R.; Tirado, J.; Bromiley, G.; Bromiley, F.; Boffa Ballaran, T. *Solid State Ionics* **2003**, *161*, 197.
(14) Albrecht, S.; Kümpers, J.; Kruft, M.; Malcus, S.; Vogler, C.; Wahl, M.; Wohlfahrt-Mehrens, M. *J. Power Sources* **2003**, *119*−*121*, 178.
(15) Guilmard, M.; Croguennec, L.; Denux, D.; Delmas, C. *Chem. Mater.* **2003**, *15*, 4476.
(16) Moshtev, R.; Zlatilova, P.; Manev, V.; Sato, A. *J. Power Sources* **1995**, *54*, 329.
(17) Arai, H.; Okada, S.; Ohtsuka, H.; Ichimura, M.; Yamaki, J. *Solid State Ionics* **1995**, *80*, 261.
(18) Rougier, A.; Gravereau, P.; Delmas, C. *J. Electrochem. Soc.* **1996**, *143*, 1168.
(19) Rougier, A.; Saadoune, I.; gravereau, P.; Willmann, P.; Delmas, C. *Solid State Ionics* **1996**, *90*, 83.
(20) Alcántara, R.; Lavela, P.; Tirado, J. *Chem. Mater.* **1997**, *9*, 2145.
(21) Alcántara, R.; Lavela, P.; Tirado, J. *J. Electrochem. Soc.* **1998**, *145*, 730.
(22) Delmas, C.; Ménétrier, M.; Croguennec, L.; Saadoune, I.; Rougier, A.; Pouillerie, C.; Prado, G.; Grüne, M.; Fournés, L. *Electrochim. Acta* **1999**, *45*, 243.
(23) Van der Ven, A.; Ceder, G. *Electrochem. Solid-State Lett.* **2000**, *3*, 301.
(24) Reed, J.; Ceder, G. *Electrochem. Solid-State Lett.* **2002**, *5*, A145.
(25) Reed, J.; Ceder, G. *Chem. Rev.* **2004**, *104*, 4513.
(26) Ma, X.; Kang, K.; Ceder, G.; Meng, Y. *J. Power Sources* **2007**, *173*, 550.
(27) Chang, C.; Velikokhatnyi, O.; Kumta, P. *J. Electrochem. Soc.* **2004**, *151*, J91.
(28) Amriou, T.; Sayede, A.; Khelifa, B.; Mathieu, C.; Aourag, H. *J. Power Sources* **2004**, *130*, 213.
(29) Chen, C.; Liu, J.; Stoll, M.; Henriksen, G.; Vissers, D.; Amine, K. *J. Power Sources* **2004**, *128*, 278.
(30) Zhong, Y.; Zhao, X.; Cao, G. *Mater. Sci. Eng., B* **2005**, *121*, 248.
(31) Sivaprakash, S.; Majumder, S.; Nieto, S.; Katiyar, R. *J. Power Sources* **2007**, *170*, 433.
(32) Yoshizawa, H.; Ohzuku, T. *J. Power Sources* **2007**, *174*, 813.
(33) Koyama, Y.; Tanaka, I.; Adachi, H.; Makimura, Y.; Ohzuku, T. *J. Power Sources* **2003**, *119*, 644.
(34) Lin, Y.; Lu, C. *J. Power Sources* **2009**, *189*, 353.
(35) Kresse, G.; Joubert, D. *Phys. Rev. B* **1999**, *59*, 1758.
(36) Kresse, G.; Furthmuller, J. *Phys. Rev. B* **1996**, *54*, 11169.
(37) Chase, M. *JANAF Thermochemical Tables*; American Chemical Society: New York, 1986.
(38) Adachi, H.; Tsukada, M.; Satoko, C. *J. Phys. Soc. Jpn.* **1978**, *45*, 875.
(39) Slater, J. *Phys. Rev.* **1951**, *81*, 385.
(40) Adachi, H.; Kowada, Y.; Tanaka, I.; Nakamatsu, H.; Mizuno, M. *Hajimeteno Denshijoutai Kaisan*; Sankyo-Shuppan: Tokyo, Japan, 1998.
(41) Kim, Y.; Kang, S. *Acta Mater.* **2011**, *59*, 126.
(42) Kim, Y.; Kang, S. *Acta Mater.* **2011**, *59*, 3024.
(43) Wang, L.; Maxisch, T.; Ceder, G. *Chem. Mater.* **2007**, *19*, 543.
(44) Ong, S.; Wang, L.; Kang, B.; Ceder, G. *Chem. Mater.* **2008**, *20*, 1798.
(45) Barber, C.; Dobkin, D.; Huhdanpaa, H. *ACM Trans. Math. Software* **1996**, *22*, 469.
(46) Inorganic Crystal Structure Database, http://icsd.kisti.re.kr/
(47) Kang, K.; Meng, Y.; Bréger, J.; Grey, C.; Ceder, G. *Science* **2006**, *311*, 977.
(48) Zhou, F.; CoCoccioni, M.; Marianetti, C.; Morgan, D.; Ceder, G. *Phys. Rev. B* **2004**, *70*, 235121.
(49) Wang, L.; Maxisch, T.; Ceder, G. *Phys. Rev. B* **2006**, *73*, 195107.
(50) Wang, L.; Maxisch, T.; Ceder, G. *Chem. Mater.* **2007**, *19*, 543.
(51) Cheralathan, K.; Kang, N.; Park, H.; Lee, Y.; Choi, W.; Ko, Y.; Park, Y. *J. Power Sources* **2010**, *195*, 1486.